

Experimental study of the binding energy of NH₃ on different types of ice and its impact on the snow line of NH₃ and H₂O

S. Kakkenpara Suresh^{1,2}, F. Dulieu¹, J. Vitorino¹, and P. Caselli²

¹ LERMA, CY Cergy Paris University, 5 mail Gay Lussac, Neuville-sur-Oise
e-mail: shreyaks@mpe.mpg.de

² Max Planck Institute for Extraterrestrial Physics, Giessenbachstraße 1, 85748 Garching, Germany

Received; accepted

ABSTRACT

Context. N-bearing molecules (like N₂H⁺ or NH₃) are excellent tracers of high-density and low-temperature regions, such as dense cloud cores. Moreover, they could shed light in understanding snow lines in protoplanetary disks and the chemical evolution of comets. However, a lot remains unknown about the chemistry of these N-bearing molecules on grain surfaces - which could play an important role in their formation and evolution.

Aims. In this work, we experimentally study the behaviour of NH₃ on surfaces that mimic grain surfaces under interstellar conditions in the presence of some of the other major components of interstellar ices (i.e. H₂O, CO₂, CO). We measure the binding energy distributions of NH₃ from different H₂O ice substrates and also investigate how it could affect the NH₃ snow line in protoplanetary disks.

Methods. We performed laboratory experiments using the Ultra High Vacuum (UHV) setup VENUS (VErs des NoUvelles Syntheses) where we co-deposited NH₃ along with other adsorbates (here H₂O, ¹³CO and CO₂) and performed Temperature Programmed Desorption (TPD) and Temperature Programmed-During Exposure Desorption (TP-DED) experiments. The experiments were monitored using a Quadrupole Mass Spectrometer (QMS) and a Fourier Transform Reflection Absorption Infrared Spectrometer (FT-RAIRS). We obtained the binding energy distribution of NH₃ on Crystalline Ice (CI) and compact-Amorphous Solid Water ice (c-ASW) by analysing the TPD profiles of NH₃ obtained after consequent depositions on these substrates.

Results. In the co-deposition experiments, we observe a significant delay in the desorption and a decrease of the desorption rate of NH₃ when H₂O is introduced into the co-deposited mixture of NH₃-¹³CO or NH₃-CO₂, which isn't the case in the absence of H₂O. Secondly, we notice that H₂O traps roughly 5-9% of the co-deposited NH₃, which is released during the phase change of water from amorphous to crystalline. Thirdly, we obtain a distribution of binding energy values of NH₃ on both the ice substrates instead of an individual value as assumed in previous works. For CI, we obtained an energy distribution between 3780K - 4080K, and in the case of amorphous ice, the binding energy values are distributed between 3630K - 5280K - in both cases using a pre-exponential factor of $A = 1.94 \times 10^{15} \text{ s}^{-1}$.

Conclusions. From our experiments, we conclude that the behaviour of NH₃ is significantly influenced by the presence of water owing to the formation of hydrogen bonds with water, in line with quantum calculations. This interaction, in turn, preserves NH₃ on the grain surfaces longer and to higher temperatures making it available closer to the central protostar in protoplanetary disks than previously thought. It well explains why NH₃ freeze out in pre-stellar cores is efficient. When present along with H₂O, CO₂ also appears to impact the behaviour of NH₃ retaining it at temperatures similar to those of water. This may impact the overall composition of comets, particularly the desorption of molecules from their surface as they approach the Sun.

Key words. Astrochemistry – ISM: molecules – Methods: laboratory: solid state – Molecular processes – Protoplanetary disks – Comets: General

1. Introduction

Ammonia is one of the six major molecules found in the solid phase in interstellar ices (Boogert et al. 2015). It has been observed in a variety of environments in the universe like comets (e.g. Poch et al. (2020)), star-forming regions (e.g., Fehér et al. (2022)), external galaxies (e.g. Gorski et al. (2018)), the centre of our galaxy (e.g. Sandqvist et al. (2017)) and in the Solar System planets. It was first detected in the interstellar medium towards the Galactic centre by Cheung et al. (1968) by its J=1, K=1 inversion transition. In dense starless clouds, where temperatures can be as low as 6K (Crapsi et al. 2007; Pagani et al. 2007) and number densities between 10⁴ - 10⁶ cm⁻³ (Keto & Caselli 2010), molecular gas tracers like CO and CS are depleted from the gas phase and mainly reside on the surface of dust grains

upon freeze-out (Caselli et al. 1999; Tafalla et al. 2002). A similar scenario (large degree of C-bearing molecular freeze-out) is expected in the mid-plane of protoplanetary disks, where number densities are orders of magnitude larger than the central regions of dense starless cores (Dutrey et al. 1997; Henning & Semenov 2013; Qi et al. 2013). However, N-bearing molecules, in particular, NH₃ and N₂H⁺ and their deuterated forms, appear to be more resilient to freeze-out (e.g. Caselli et al. (2002), Tafalla et al. (2002), Tafalla et al. (2004), Crapsi et al. (2007)). For this reason, they are considered excellent tracers of dense and cold interstellar regions. More recent work, using multi-transition studies done with the IRAM 30m antenna and high sensitivity interferometric observations with ALMA and JVLTA, has shown that these molecules freeze out within the central region of pre-

stellar cores (e.g. Redaelli et al. (2019), Caselli et al. (2022), Pineda et al. (2022)), although at higher densities than CO. Gas-grain astrochemical models are now able to reproduce the observations (Caselli et al. 2022; Pineda et al. 2022). Still, they are limited by uncertainties in certain factors like the binding energies of NH_3 and knowledge of its surface chemistry. Following the work of Collings et al. (2004), Penteado et al. (2017) derived binding energies for several species, including NH_3 . Similarly, Collings et al. (2004), He et al. (2016) and Suhasaria et al. (2015) have studied the desorption properties of NH_3 from various substrates. However, the binding energies of NH_3 , the importance of surface chemistry for its formation, and its chemical desorption efficiency (Caselli et al. 2017; Sipilä et al. 2019) can be better constrained.

Ammonia has been shown to be stored efficiently in the form of ammonium salts by Kruczkiewicz et al. (2021), which at higher temperatures decompose to release ammonia into the gas phase irrespective of the presence or absence of water. This release into the gas phase occurs at a temperature higher than that of the desorption of water ice (Temp $\sim 154\text{K}$) but lower than room temperature. This implies that ammonia could be found closer to a young stellar object than the water snow line. The majority of NH_3 in molecular mantles should therefore be free to interact with the major components of interstellar or cometary ices such as water, CO_2 or CO. Similarly, Poch et al. (2020) have demonstrated that ammonium salts are a dominant nitrogen-reservoir on cometary surfaces, explaining the low measured cometary nitrogen-to-carbon ratio as compared to that of the Sun. Finally, as ammonia ice is one of the major nitrogen reservoirs in star-forming regions (Öberg et al. 2011), knowledge of the ammonia snow line is crucial while considering the formation and evolution of more complex N-bearing species in planetary systems.

The aim of this work is to study the behaviour of ammonia in the presence of the different components of molecular ice mantles like H_2O , CO and CO_2 . We, then, performed studies to obtain the binding energy of ammonia on different water ice substrates, namely c-ASW and CI. Additionally, we conducted experiments to determine the snow line of ammonia. The article is organised as follows: Section 2 describes the experimental set-up; section 3 details the experiments and the results; section 4 discusses the conclusion and section 5 outlines the discussion and future prospects.

2. Experimental Set-up

The experiments are performed on the VENUS (VErs de NoUvelles Syntheses) setup, allowing us to reproduce the conditions in cold, dark clouds (Congiu et al. 2020). VENUS consists of an ultra-high vacuum (UHV) chamber - that can attain a base pressure of 1×10^{-10} hPa (1 hPa = 1 mbar) - and five independent beams (which can be used simultaneously to inject the desired species). A Quadrupole Mass Spectrometer (QMS) and the beam of a Fourier-Transform Reflection Absorption Infrared Spectrometer (FT-RAIRS) are also present in the UHV chamber (hereafter referred to as the main chamber) that can be used to make qualitative and quantitative measurements during experiments. Depositions are made on a polycrystalline gold substrate - enclosed within the main chamber - which is chemically inert and acts as a proxy surface to dust grains for species adsorption/desorption for reactions. This surface is attached to the cold head of a closed-cycle He cryostat, which allows the surface temperature to be varied between 10 - 400K. Four of the five beams are separated from the main chamber via two inter-

mediary chambers - 1 and 2. These intermediary chambers are responsible for regulating the pressure of the injected species between the four beams ($p \sim 10^{-5}$ - 10^{-4} mbar) and the main chamber via differential pumping. The four beams are labelled: the top beam, the central beam, the right beam, and the bottom beam. For the experiments in this paper, only the first three beams are used. The fifth beam is attached to the main chamber and can inject species directly into the chamber (also known as *background deposition*).

3. Results

3.1. Co-deposition experiments

The initial set of experiments aims to understand the interaction of ammonia with the major components found on the grain mantles, as mentioned earlier. Our work considers three major molecules: H_2O , CO, and CO_2 . However, for our experiments, we use ^{13}CO (mass = 29 amu) instead of ^{12}CO (mass = 28 amu) to allow clear distinction from atmospheric N_2 (mass = 28 amu) by the QMS. Similarly, the major mass channels for water is 18 amu and that of NH_3 is 17 amu. However, water also has fragments of mass = 17 amu and NH_3 fragments into mass = 16 amu. To distinguish between these overlapping fragments of H_2O and NH_3 , we independently perform experiments using each species, determine the ratio/percentage of fragmentation into each mass by the QMS and calibrate the quantities for each mass proportionately. Initially, we co-deposit ammonia with each of these components separately. We inject the species onto the gold substrate, maintained at a temperature of 10K during the deposition. Each of these species is dosed using separate beams. A laser beam is used to ensure that every beamline overlaps on the same spot on the deposition substrate. The details of the alignment process can be found in Congiu et al. (2020) and have been omitted here for brevity. The pressure of the NH_3 , ^{13}CO and CO_2 at first stage of the beam is a few 10^{-5} mbar (corresponding to a flux: 0.1 sccm^{-1}) while that of H_2O is roughly 4.8×10^{-5} mbar. We define a monolayer as 1×10^{15} molecules cm^{-2} . The reproducibility between two depositions is within a few per cent and the accuracy in the absolute determination of an ML is around 20% since it is more precise for some molecules and less for other species (like NH_3). Table 1 lists the experiments used for the co-deposition experiments along with the ratios and monolayers of each species used. The raw data (mass spectra as well as IR spectra) are accessible online via a dedicated database². We have also carried out and analysed other sets of experiments under similar conditions listed in Appendix A, which should be accessible online. For this article, we selected the experiments that best demonstrated our findings.

The inset in Fig. 1 represents the TPD of 1ML NH_3 on a gold substrate maintained at 10K and is used to calibrate all the experiments. In the calibration experiment, to determine the dose for 1ML, we performed a series of TPDs with various doses of NH_3 on a gold substrate held at 10K and a flux of 0.1 sccm in the injection chamber. We found that 1ML of NH_3 is deposited after ~ 9 min of deposition. The ramp for all the experiments is 0.2K/s . The details of the calibration can be found in Appendix B.

Fig. 1 shows the TPD curves of the NH_3 - H_2O co-deposition experiments. In the calibration experiment, we observe a sudden rise in the NH_3 desorption around 80K which falls off

¹ sccm = standard cubic centimetre

² <https://lerma.labo.cyu.fr/DR/traitement.php>

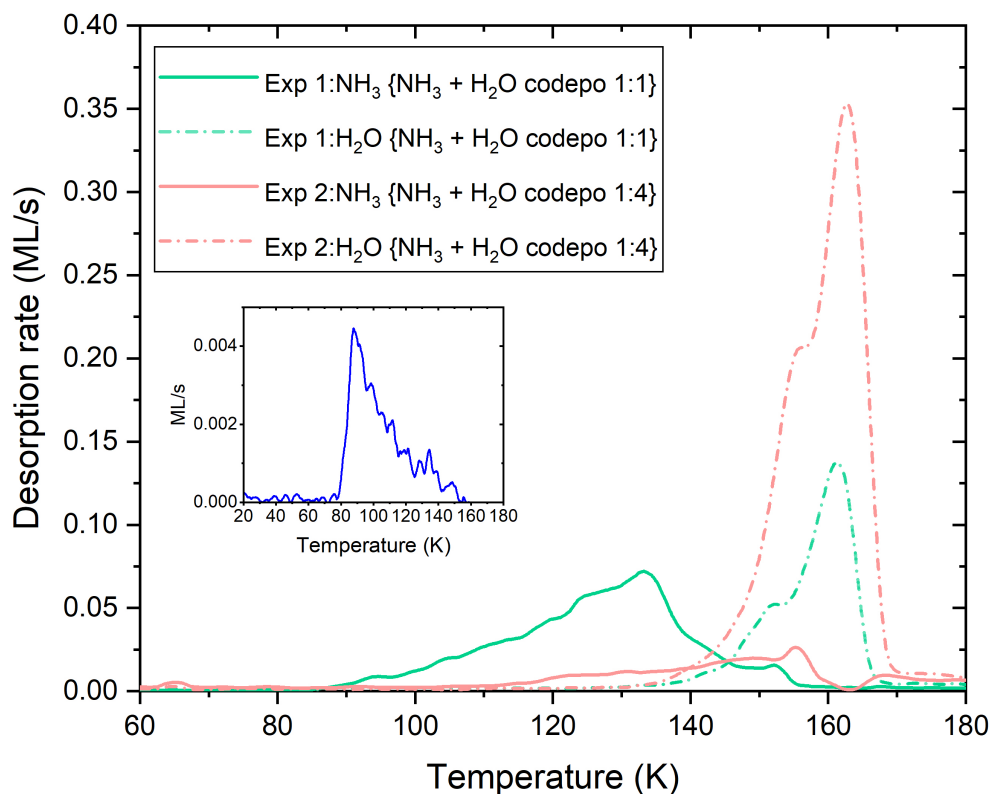


Fig. 1: NH₃-H₂O co-deposition experiments. All experiments have been performed on a gold substrate. The TPDs have a ramp of 0.2K/s. The solid lines represent the desorption of NH₃ while the dashed-dotted lines represent the desorption of water. Lines of the same colour belong to the same set of experiments. Inset: TPD of NH₃ from a gold surface used to calibrate all the consequent experiments.

slowly once peak desorption has been completed. Contrarily, during the co-deposition with water, we observe a significant decrease of the NH₃ desorption rate, and peak desorption shifted to higher temperatures. We find that about 6% w.r.t to H₂O of the deposited NH₃ is trapped by water and then released during the phase change of water from amorphous to crystalline. This trapped fraction is estimated by calculating the area under the TPD profile of the desired species (in this case NH₃). In reality, water deposited at such low temperature is fairly porous and, hence, has a larger surface area wherein the NH₃ molecules can lodge themselves. As the temperature is raised, water undergoes a phase change from amorphous to crystalline which can be observed as the plateau/shoulder at around 155K in the desorption curve of water (Fig. 1, see also Speedy et al. (1996)), as well as a change in the IR spectra (not shown here). During this phase change, water molecules begin to re-arrange to form a crystalline structure during which it pushes out any NH₃ in its bulk. Furthermore, the higher the H₂O/NH₃ ratio, the more the desorption of ammonia is delayed - as expected. Indeed, when the NH₃ concentration is very high, there are more NH₃-NH₃ interactions which can substitute for NH₃-H₂O interactions.

During the TPD of the co-deposition experiments of NH₃-¹³CO mixture (Fig. 2), NH₃ desorbs independently (top row Fig. 2a and 2b) of ¹³CO, irrespective of the ratio between the two. All of the NH₃ is desorbed between 80K-132K. The desorption is in good agreement with a fit to the desorption rate equation

$A \times \exp(-E/k_b T)$, where E/k_b is the binding energy (in Kelvins), T is the temperature (in Kelvins) and A is the pre-exponential factor (s^{-1}). Since these experiments are in the multilayer regime (zero order kinetics), we chose $E/k_b = 2965K$ and the $A = 2.1 \times 10^{12} s^{-1}$ following Martín-Doménech et al. (2014) and assuming that $1ML = 10^{15}$ molecules cm^{-2} . The offset from the fit seen in 2b is due to the low quantities of NH₃ used for the experiments. Higher quantities would ensure a good fit as in the previous case.

When present with NH₃ in equal quantities, 85.8% of the deposited ¹³CO is desorbed between 20K-50K (Fig 2c middle row orange curve). At the same time, ¹³CO exhibits a volcano effect due to NH₃. A volcano effect is the sudden desorption of a volatile species trapped under a less volatile species like H₂O when the latter begins to desorb (Smith et al. (1997), Viti et al. (2004), Collings et al. (2003)). This volcano effect can be observed as the peak between 68K-80K and accounts for ~ 9% of the total desorbed ¹³CO. On the contrary, this trapping is not observed when NH₃ is present in trace quantities, as expected (Fig 2d). The ¹³CO peak between 90K-110K is the CO desorbing with NH₃. This is probably the CO adsorbed on the substrate during the initial moments of the co-deposition and thereby buried under the later layers of NH₃ and ¹³CO. The right panels of Fig. 2 contain the experiments in proportions that are more astronomically relevant. Hence, here, NH₃ is deposited in trace amounts (1 ML or sub-monolayer quantities) as compared to ¹³CO and H₂O. Once again, for NH₃, we observe a similar desorption trend as in the case of the experiments presented in Fig. 1.

Table 1: List of co-deposition experiments.

No.	Experiment	Ratio	Quantity deposited (ML)
1	{NH ₃ + H ₂ O}	1:1	~10 ML of each
2	{NH ₃ + H ₂ O}	1:4	5.8 (NH ₃), 23.8(H ₂ O)
3	{NH ₃ + ¹³ CO}	1:1	11.3(NH ₃), 12.3(¹³ CO)
4	{NH ₃ + ¹³ CO}	1:6	1(NH ₃), 6.5(¹³ CO)
5	{NH ₃ + ¹³ CO + H ₂ O}	1:1:1	8.1(NH ₃), 9.2(¹³ CO), 9.2(H ₂ O)
6	{NH ₃ + ¹³ CO + H ₂ O}	1:2:9	1.6(NH ₃), 3.6(¹³ CO), 8.9(H ₂ O)
7	{NH ₃ + CO ₂ }	1:1	14.7(NH ₃), 14.7(CO ₂)
8	{NH ₃ + CO ₂ }	1:7	0.7(NH ₃), 5.4(CO ₂)
9	{NH ₃ + CO ₂ + H ₂ O}	1:1:1	9(NH ₃), 9.3(CO ₂), 8.9(H ₂ O)
10	{NH ₃ + CO ₂ + H ₂ O}	1:4:5	1.5(NH ₃), 4(CO ₂), 5.5(H ₂ O)

Note: All experiments are performed on a gold substrate held at 10K. The ratios have been rounded off to the nearest whole number for visual convenience while the no. of mono-layers deposited has been mentioned to one decimal point of accuracy. The ramp during the TPD is 0.2K/s. Additional experiments have been carried out but not included in the main article for brevity and can be found in Appendix A.1

In the presence of H₂O, the trend in the desorption of NH₃ and ¹³CO is different as a significant delay in the desorption of NH₃ is observed. When present in quantities roughly equal to water, the NH₃ desorption rate is slower and the desorption is delayed compared to its desorption in the absence of water. In the multi-layer (Fig. 2a) and the sub-monolayer (Fig. 2b) scenario, the NH₃ desorption is shifted to higher temperatures. In the former, NH₃ desorption is delayed possibly because it needs to diffuse through the bulk of the ice before desorption can take place. In the latter, at low concentrations there is a higher probability for greater NH₃-H₂O interaction and lower NH₃-NH₃ interaction via hydrogen bonds resulting in water holding on to NH₃ for a little longer than when NH₃ is present in larger quantities. It is worth noting in both cases that an NH₃ volcano peak is observed due to the crystallisation of water. Roughly 5% of NH₃ w.r.t water is trapped by water when co-deposited in equal quantities and around 8.5% is trapped by water in the more astrophysically relevant scenario (Expt 6 in Table. 1) where it is released, as observed in previous experiments, during the change of phase of H₂O from amorphous to crystalline.

The co-deposition experiments of NH₃ with CO₂ also exhibit a similar behaviour as for CO ones. NH₃ desorption appears to be unaffected by the presence of CO₂ (Fig.3a and 3b). NH₃ desorbs

in the same temperature range as previously observed for experiments with ¹³CO. Its desorption fits well the curve of desorption rate equation mentioned earlier with the values taken from Martín-Doménech et al. (2014). When the two are in equal quantities (Fig. 3b), the bulk of CO₂ desorbs between 70K-92K. 2% of the deposited CO₂ desorbs during the desorption of NH₃. This could be due to mechanical trapping by NH₃, and hence the former could desorb only after all the NH₃ desorbed. The shift in peak desorption temperature of NH₃ towards higher values observed in Fig. 3b as compared to Fig. 3a is due to the fact that in the former we have multiple layers of NH₃. Additionally, in the sub-ML experiments (Fig. 3a, c and e), we use very low quantities of NH₃ and therefore, the interaction between NH₃ and the gold in the substrate becomes significant. Once again, the presence of H₂O seems to significantly alter the desorption of both NH₃ (Fig. 3a and b) and CO₂ (Fig. 3c and d). NH₃ desorbs in a similar manner to the previous experiments with ¹³CO. Its desorption is not only delayed but the rate is also slower. Roughly 9% of it is trapped and then released during the phase change of H₂O. CO₂ desorption, on the other hand, doesn't appear delayed. However, roughly 2% of it is trapped by water and then released along with NH₃ during the phase change of H₂O. In previous experimental works, Bossa et al. (2008) and Noble et al. (2014)

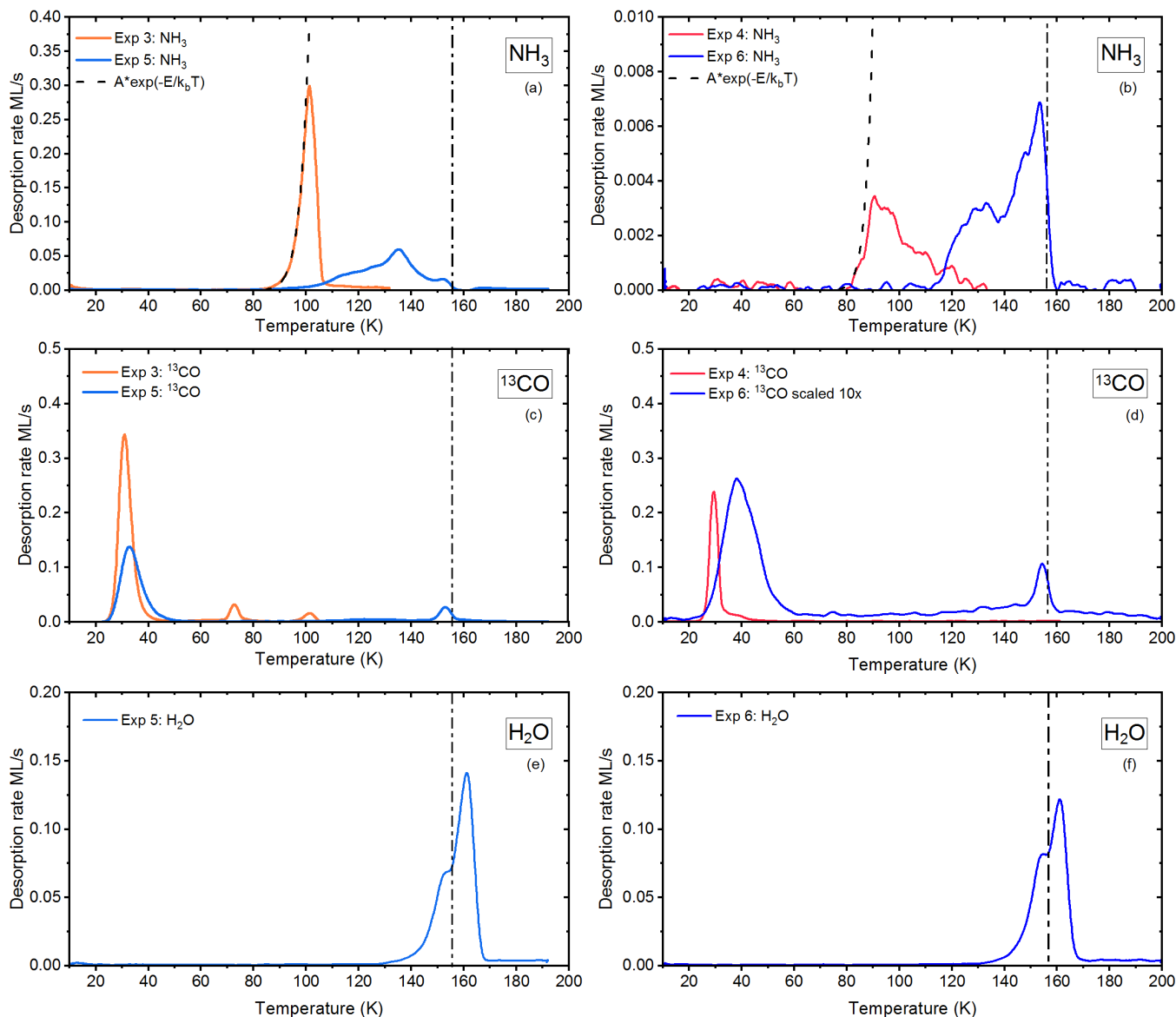


Fig. 2: NH₃-¹³CO (and H₂O) co-deposition experiments. The mass channels used for H₂O, NH₃ and ¹³CO are 18 amu, 17 amu, and 29 amu, respectively also accounting for fragments of mass = 17 amu (for H₂O) and 16 amu (for NH₃). All experiments have been performed on a gold substrate. The TPDs have a ramp of 0.2K/s. Lines of the same colour belong to the same set of experiments. The dash-dot vertical line at 155K corresponds to the temperature of the phase change of water from ASW to crystalline.

have shown that carbamic acid (NH₂COOH) can be formed as early as 80K by thermal reaction of CO₂ and NH₃. We do not observe this reaction in our experiments - which are performed in much thinner layers - probably because this reaction only occurs if the reactants are solvated. Similarly, [Potapov et al. \(2019\)](#) reported the formation of NH₄⁺NH₂COO⁻, which we do not observe in our experiments.

3.2. Desorption of NH₃ from different types of ices

A second set of experiments is performed to understand the desorption dynamics and determine the distribution of binding energies. The method used has been discussed in more detail in [De Jong & Niemantsverdriet \(1990\)](#), [He et al. \(2011\)](#) and [Amaud \(2006\)](#). Subsequent depositions of roughly 1 ML of

NH₃ are made on each type of ice substrate followed by a TPD. Two kinds of ice substrates are used for this purpose: crystalline ice and compact amorphous solid water ice. The crystalline ice substrate is formed by depositing water onto the deposition surface held at 110K followed by flash heating up to 150K. To create a compact amorphous water ice substrate, water is deposited onto the gold substrate at 110K and an incident angle of $\theta = 0^\circ$ with respect to the normal of the gold substrate. A normal angle of incidence leads to a denser ice substrate as shown by [Kimmel et al. \(2001a,b\)](#). Several studies have shown a key role between the deposition temperature and its effect on the ice substrate. [Scott Smith et al. \(2006\)](#) found that water deposited at ≤ 110 K is amorphous but already begins to pre-crystallise at ≥ 120 K since it is thermodynamically favoured. [He et al. \(2019\)](#) and [Bossa et al. \(2012\)](#) observed a significant reduction in the

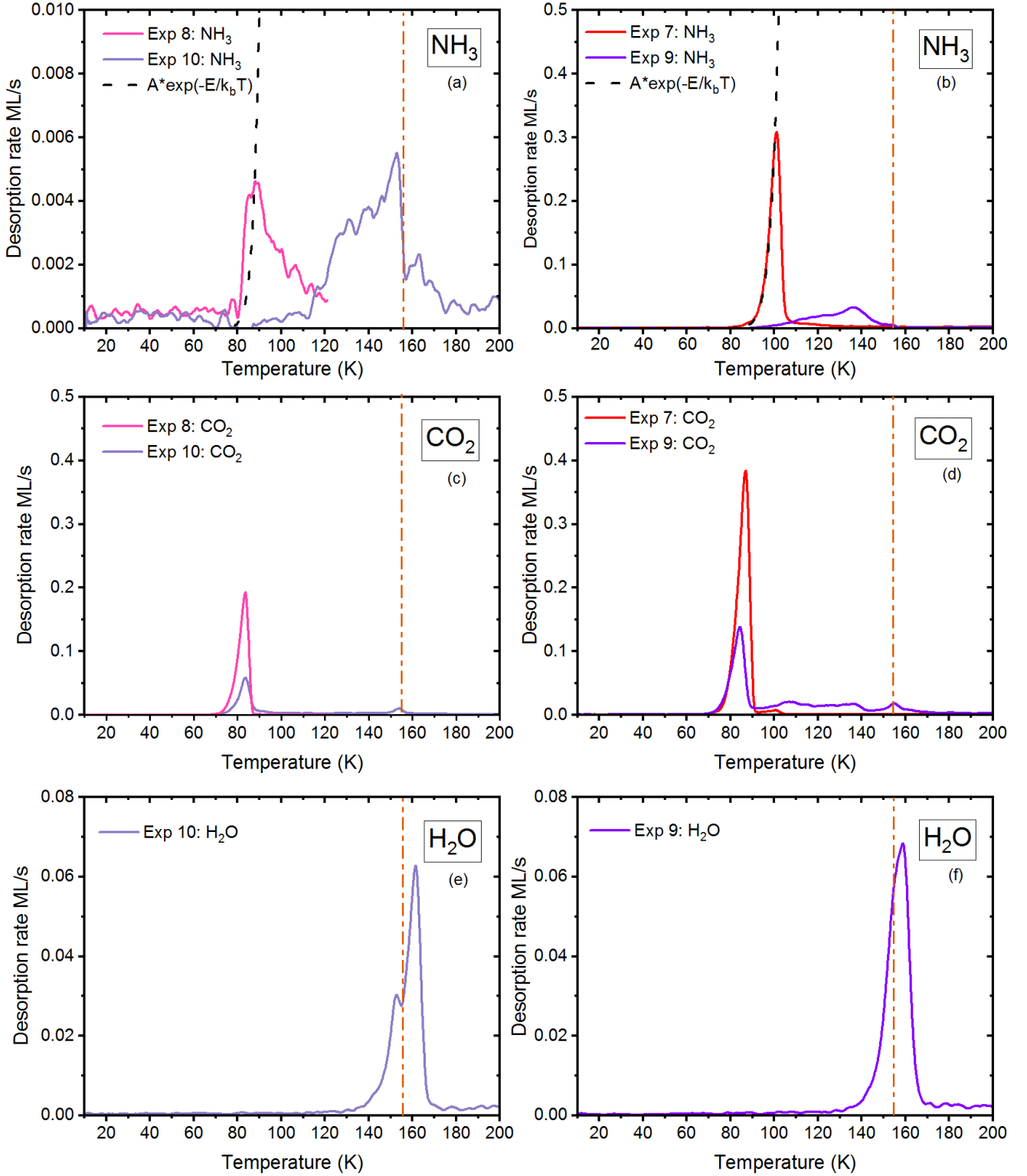


Fig. 3: Same as Fig 2 but using CO_2 instead of ^{13}CO . The mass channel used for CO_2 is 44 amu.

porosity of the substrate beyond 100 K. Both these studies are performed on samples that are ~ 200 MLs and ~ 3000 MLs, respectively, while the present study focuses on thin ices (\sim tens of MLs). Hence is safe to assume that the amorphous substrate formed in our case is, indeed, compact.

To prepare the raw data for analysis, an initial adjacent averaging smoothing process employing 35 data points is applied using Origin software. This initial smoothing is carried out to reduce background noise which becomes significant at low dosages and high temperatures. Subsequently, the smoothed data is fed into a custom software developed at LERMA, which

fits a set of 19 independent TPD curves distributed evenly over a range of 19 binding energies spanning from 3030 K to 5730 K. For a more comprehensive explanation of this method, please refer to Chaabouni et al. (2018). In our analysis, we used a pre-exponential factor, A , with a value of $1.94 \times 10^{15} \text{ s}^{-1}$, as per the findings of Minissale et al. (2022). The results are presented in the form of blue curves, representing the mass spectrometer data, and orange curves, representing the fit to the experiments conducted using software developed within our laboratory.

NH₃ on CI (Fig. 4) desorbs in a manner similar to NH₃ on the gold substrate as in the calibration experiments. There is a sharp increase in the desorption rate at 75K. Most of the desorption occurs between 78K and 140K. On CI, we observe two peaks. The first one (between 76K - 98K) is the multi-layer desorption of NH₃ due to its interaction with itself rather than with the surface and does not necessarily need full layers of NH₃ to be present to appear. The second one is between 98K - 112K and we observe an increase in the height of this peak with each deposition. This implies that the surface evolves with each cycle of dosing the crystalline surface with NH₃. In other words, NH₃ is able to amorphise the surface structure of the ice by introducing defects onto its surface. This modification seems, however, to be a surface phenomenon and alters only the top layers of the surface. Even when the quantity of NH₃ is increased, NH₃ prefers to bind to H₂O than with itself as is evident by this observed increase in peak height in Fig. 4. Nevertheless, this modification doesn't affect the desorption of either H₂O or NH₃ as the latter is eventually pushed out of the surface of CI during the desorption of water. This, in turn, renders it harder to calculate one single value of binding energy for NH₃ on CI.

He et al. (2016) conducted a similar investigation in which they deposited NH₃ onto a CI substrate to determine the binding energy of NH₃ desorption. Our study exhibits considerable resemblance with their research, particularly with respect to their TPD curve obtained for a deposition of 2ML. Noticeably, a major proportion of the desorption events in both studies occur within the temperature range of 80 K to 145 K. However, a discrepancy arises in the temperature at which the multilayer desorption peak is observed. He et al. reported this peak occurring at a slightly elevated temperature, approximately 100 K. This difference could potentially be attributed to their use of a higher heating ramp rate, estimated to be around 0.5 K/s, during their TPD experiments. Another distinguishing feature between the two studies pertains to the temperature of complete desorption of the ices. In our investigation, it was observed that the ices are nearly completely desorbed by 140 K, whereas He et al. noted the presence of desorption signals persisting beyond 140 K. Unfortunately, a more comprehensive comparison is hindered by the lack of specified units for the desorption rate in the pertinent figure within their study. But the difference in heating speed is certainly the main difference, since the slower the heating, the earlier the desorption, for an equivalent quantity. In terms of the determination of binding energies (BE), He et al., adopting the direct inversion method, reported BE values falling within the range of approximately 2900 K to 4100 K. Notably, these BE values are lower than the values obtained in our study. This variance in BE values may be attributed to the use of a lower pre-exponential factor, specifically 10^{12} s^{-1} , in their methodology as compared to the one employed in our study. Using the conversion formula proposed in Chaabouni et al. (2018), reported in the review of Minissale et al. (2022),

we find a good agreement.

In contrast, the desorption of NH₃ on c-ASW (Fig. 5) occurs at higher temperatures. This delay could be associated with the structure of c-ASW i.e., due to the presence of concavities at the molecular level on its surface where NH₃ can lodge itself and be surrounded by many water molecules and hence form more hydrogen bonds than in the case of CI. We observe a single broad peak, which is in contrast to what we observe with CI. A bulk of this desorption occurs between 95 K and 140 K. On crystalline ice, we obtained the binding energy between two mono-layers of ammonia in the range of 3180K- 3630K and between ammonia and the surface of the water substrate in the range of 3780K – 4080K. On c-ASW, we obtained binding energy values between 3630K and 5280K. Our BE values are in very good agreement with the values obtained on ASW ice via theoretical calculations by Tinacci et al. (2022) who also used the same value of the pre-exponential factor. We also note that in experiments as well as calculations, binding energy distributions are important, and have a very good match with Germain et al. (2022). A more detailed discussion between the comparison of experiments and calculations derived values can be found in (Ferrero et al. 2022).

3.3. Temperature Programmed-During Exposure Desorption (TP-DED) experiments

Fig. 6 shows the basic schematics of a TP-DED experiment using the example of pure NH₃ deposition. For this set of experiments, the desired species is deposited onto the gold substrate Fig. 6a. simultaneously while the latter is heated/cooled at a constant ramp of 0.5K/min. During the heating process, as the deposition progresses, the species continues to accumulate/adsorb on the substrate 6b. until the desorption temperature range of the former is reached. At this point, the species begins to slowly desorb from the substrate, and any incoming molecule of the species desorbs immediately 6c. until no more incoming molecules can adsorb due to the temperature of the surface being higher than the desorption temperature 6d. The reverse is true during the cooling process. The experiment is monitored using the FT-RAIRS during the deposition and is usually followed by a TPD at the end. The details of each experiment are given in Table 2. Here, this rather rarely used type of experiment aim at mimicking snow line regions where both accretion and depletion on grains (i.e. sticking and desorption), are taking place simultaneously. A snow line is defined in a region with a thermal gradient that applies on the grains (i.e., hotter towards the star and cooler in the outer regions) such that there exists a frontier zone (the snow line) where the accretion compensates for the desorption. Towards the colder side, the accretion dominates and the molecules condense onto the grains whereas on the hotter side the concerned species are in the gas phase. Our goal is to investigate the snow line of NH₃. The results of the experiments can be found in Fig. 7.

Our study plots the area under the IR peak at 3383 cm^{-1} of NH₃ against temperature. The areas are calculated using the vibrational spectroscopy software 'OPUS' by the company BRUKER. We apply a baseline correction where necessary. It is important to mention that in experiments 2 and 3, due to heavy baseline distortion and the fact that the IR peaks of NH₃ were superimposed with that of H₂O, we were obliged to make gross assumptions to obtain the IR area of NH₃. The area we report is, hence, the area of NH₃ subtracted from the combined areas of NH₃ and H₂O.

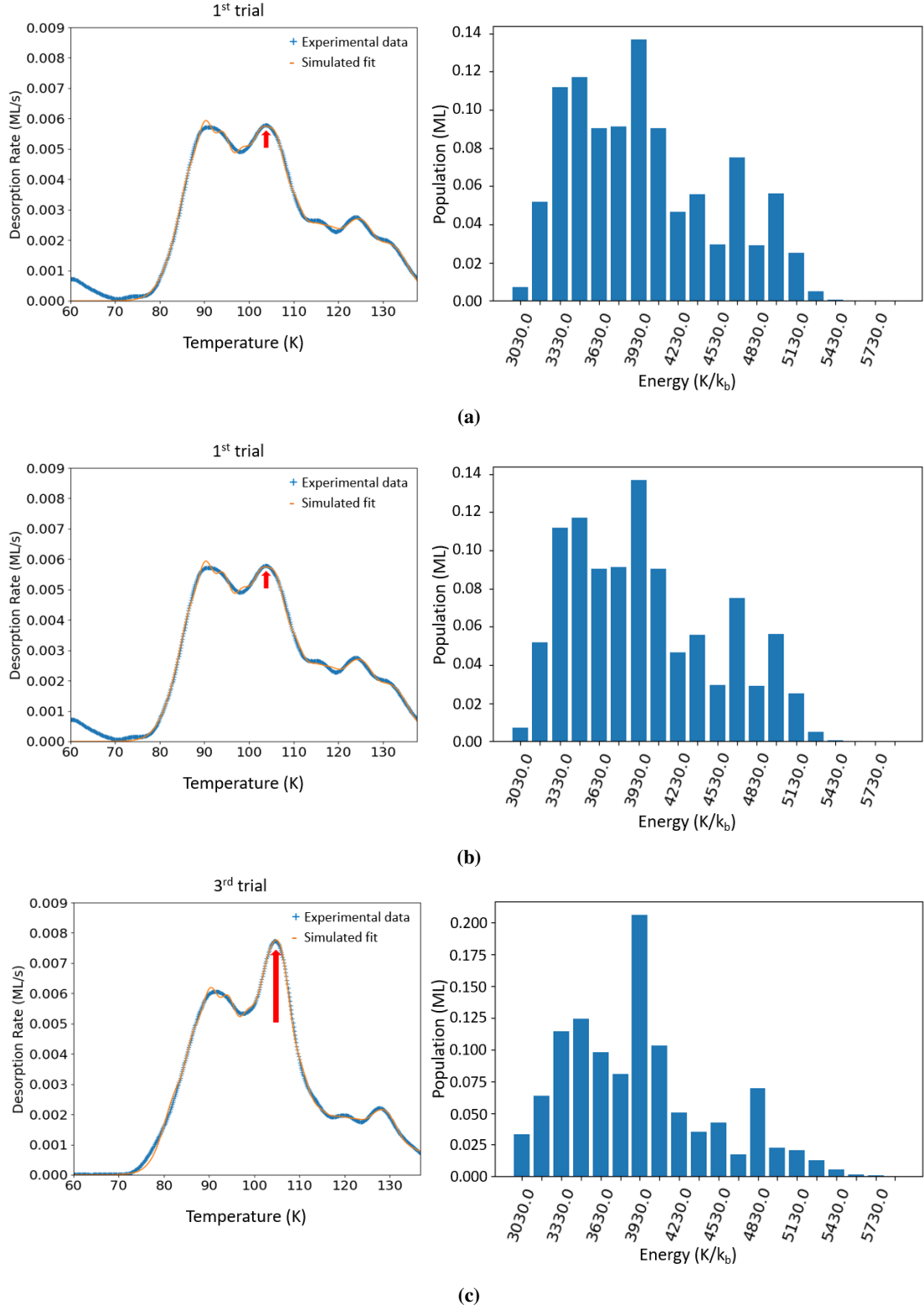


Fig. 4: Binding energy fits of the TPDs (*left column*) and the corresponding binding energy distribution histograms (*right column*) of three separate, subsequent depositions of 1 ML of NH₃ on the surface of crystalline ice. Each deposition is followed by a TPD to remove the ammonia deposited on the ice substrate before the consequent deposition is made. The preference of ammonia to bind to water instead of itself is seen as the progressive increase in peak height (indicated by the red arrow) with each trial.

All three experiments (Fig. 7a, 7b and 7c) show distinct zones during the TP-DED. In the first experiment Fig. 7a, Zone A corresponds to the accretion of NH₃ in the amorphous form. Given the time to form 1ML on the gold substrate, the signal

before 60K corresponds to NH₃ on the substrate. Beyond this temperature, the signal observed is of NH₃ on this NH₃ layer. Since the surface is continuously exposed to gaseous NH₃ and the desorption is negligible for these temperatures, ammonia

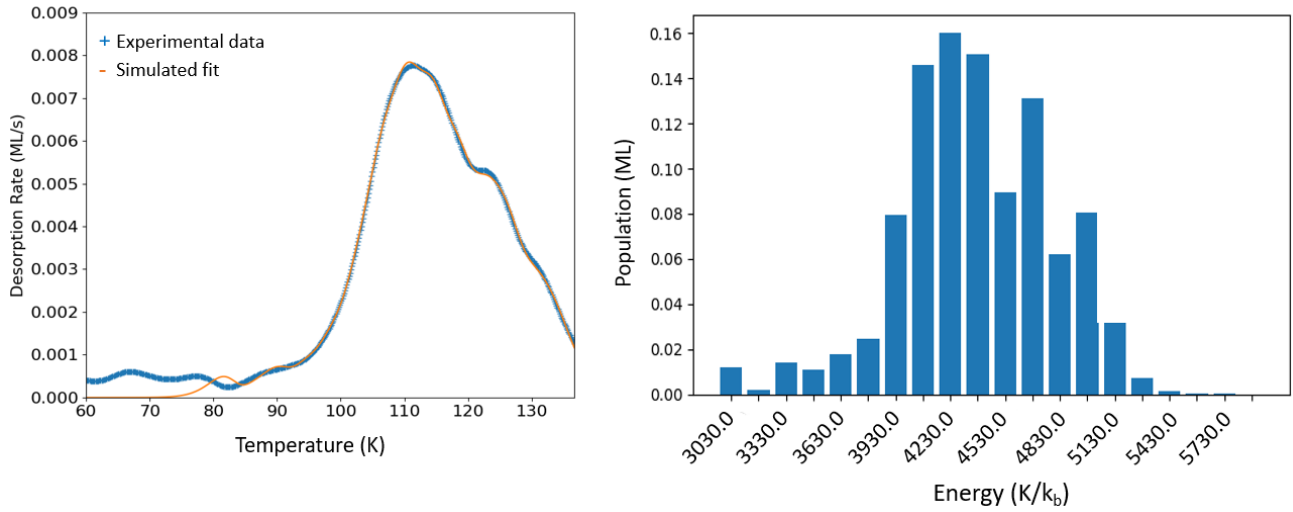


Fig. 5: Binding energy fit (*left panel*) for 1ML deposition of NH₃ on c-ASW ice and the corresponding binding energy histogram (*right panel*).

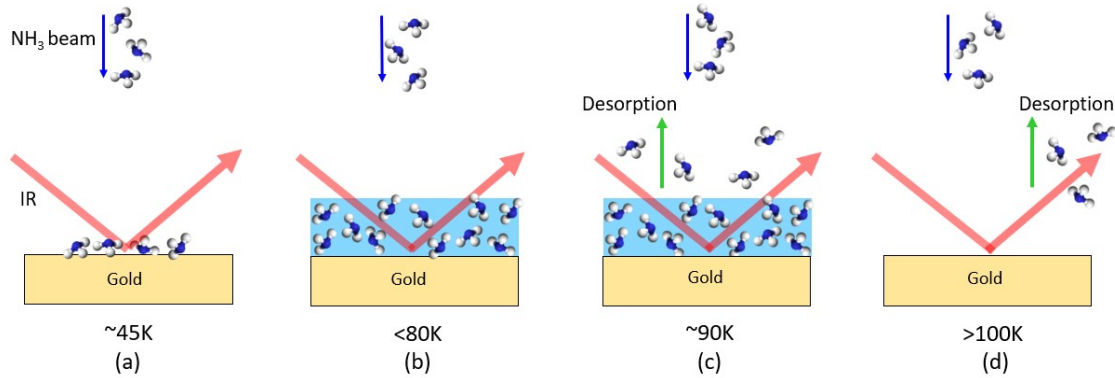


Fig. 6: Schematic explaining the sequence of events in the TP-DED experiment. Here, we use the example of an NH₃ beam but the same procedure follows for all three TP-DED experiments performed in this work. The temperatures in each sub-figure in the schematic are merely indicative due to the flux dependence of the adsorbate and not the unique temperature at which the events take place.

Table 2: List of TP-DED experiments

Expt No.	Adsorbate	Temperature Range (K)
1	NH ₃	40 - 105 105 - 94
2	NH ₃ + H ₂ O	40 - 180 180 - 60
3	NH ₃ + H ₂ O + CO ₂	40 - 180

accumulates on the surface, and we observe a linear increase in the IR absorbance signal. The same trend would be observed for a constant surface temperature desorption. As the temperature rises, NH₃ begins to change its structure from amorphous to crystalline, denoted as zone B and can be identified by a change in the slope. This is not due to a change in the flux of accretion - which is stable during every experiment - but is due to an increase in the absorption band strength after the phase

transition. This phenomenon is also observed in [Cazaux et al. \(2021\)](#), where a similar change is found during the heating of H₂S.

Around 81.5K, we notice a slowing down of the rise, followed by a plateau (Zone C). Even though the desorption rate of NH₃ increases exponentially, it is in competition with the accretion rate. As a result, a part of the molecules adsorbed is now desorbing, and thus the net accumulation slows down to almost null at the snow line - which is the turning point of the curve at around 88K. Above 90K, we notice a sudden drop in the NH₃ desorption (zone D). Here, despite the accretion, desorption still dominates. This occurs since there is no more measurable NH₃ on the surface as the adsorbed ammonia is desorbed quickly after adsorption, which is even faster in a laboratory measurement time frame.

We then perform a co-deposition of NH₃ with H₂O (see [Fig.7b](#)) under similar conditions. The first striking observation is the absence of the region of phase change of NH₃ from amorphous to crystalline. This could be due to the aforementioned preference of NH₃ to form hydrogen bonds with H₂O than with itself. Hence, zone E could be considered as the region

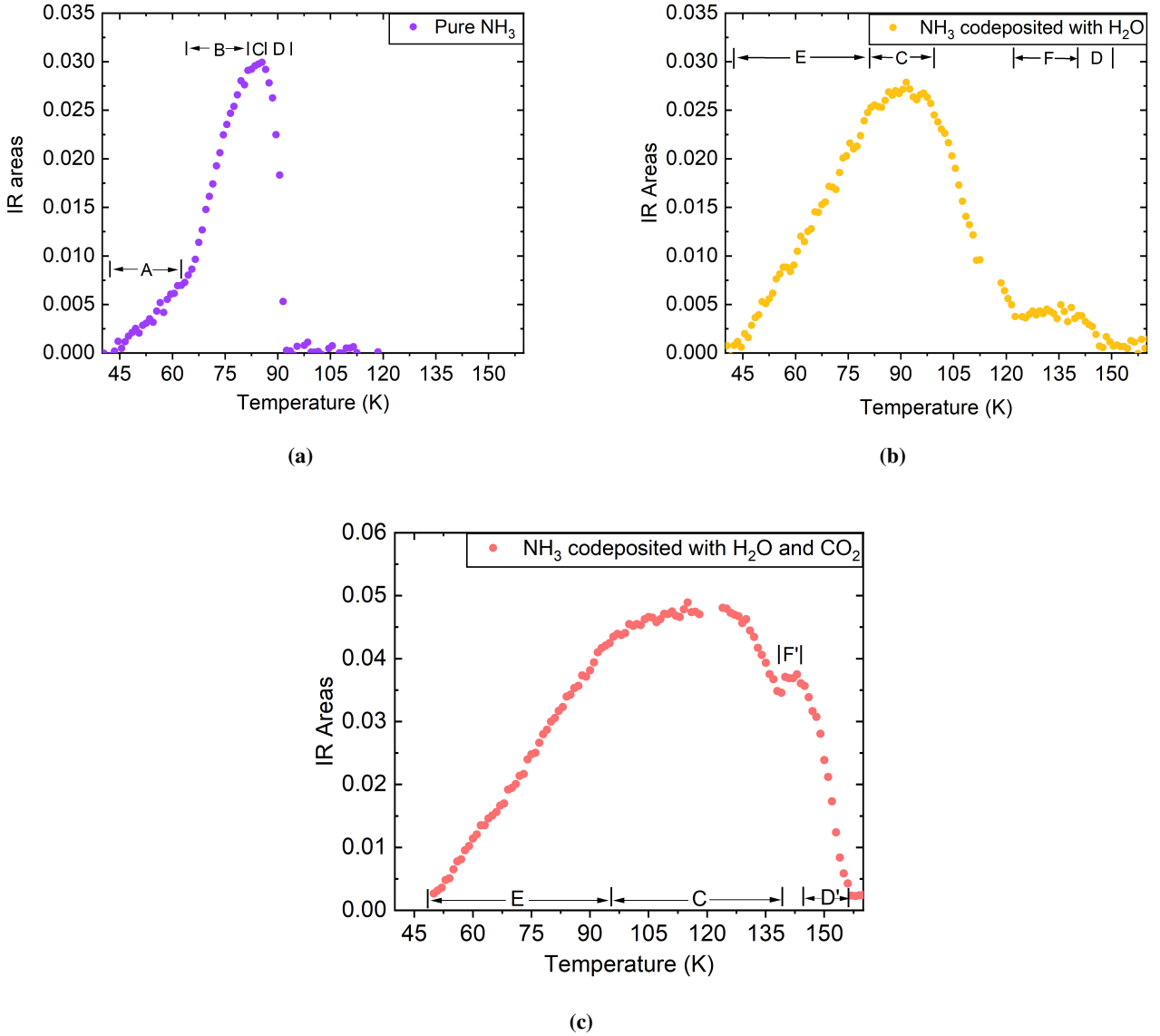


Fig. 7: Figure depicting the quantity of NH₃ deposited, with respect to temperature (K), during the TP-DED experiments measured using a FT-RAIRS. For details on the zones A, B, C, D, D', E, F AND F', refer to main text Section 3.3

that contains NH₃ within the H₂O structure. The turn-off point between zone E and zone C is less pronounced than in the previous case and marks desorption of NH₃ in interaction with itself and probably not the water ice. After roughly 105K, there is a decrease in the quantity of NH₃ due to the substrate reaching a higher desorption flux of NH₃. However, an interesting point to note here is that there still is a significant quantity of NH₃ left on the surface. This can be verified by the plateau (zone F) which is an indicator of NH₃ in H₂O. This is due to the trapping phenomena observed earlier by H₂O which is further strengthened by the NH₃-H₂O interaction. The slow decrease in the slope in zone D is the release of NH₃ due to the desorption of H₂O as the latter approaches its crystallisation temperature.

In the next set of experiments (Fig.7c), we add CO₂ to this mixture. During the experiment, we perceive a similar trend to that of the previous experiment with H₂O at the beginning of the desorption process i.e., the sudden change in the curve for NH₃ is very subtle, if at all present (zone E). The accretion

continues until the mixture reaches around 97K. At this temperature, we begin to recognise some similarities noted in the previous two experiments. Firstly, the signal of the solid NH₃ is characterised by a plateau (zone C) due to the competition between NH₃ accretion and desorption. This is followed by a sudden yet short phase in the quantity of NH₃ owing to the high temperature. Zone F marks the narrow plateau due to the NH₃-H₂O-CO₂ interaction. It is interesting to note that the quantity of NH₃ (in other words, the IR area) in this zone is significantly higher than in the previous two cases. This could point to an additional interaction of NH₃ with CO₂ that retains NH₃ until a higher temperature. However, the most interesting point to note between all three experiments is the progressive shift in the peak desorption temperature of NH₃ as we add each new species to pure NH₃ - especially in the presence of H₂O, and even more so with the addition of CO₂. There is still some NH₃ in the solid phase at unexpectedly high temperatures. In the case of NH₃/CO₂/H₂O mixture, the snow line (the turning point of NH₃) coincides with the beginning of the desorption of

water, almost superimposing their snow lines. This also raises a question about the potential role of CO₂ in the desorption of NH₃. These experiments directly demonstrate that NH₃ lacks a snow line of its own when combined with H₂O (and potentially CO₂) which, as a consequence, retains the NH₃ molecules on the grain to higher temperatures than previously expected and therefore, in a different spatial zone (the same as water).

4. Conclusions

Nitrogen-based molecules have been found in the densest parts of the interstellar medium - like pre-stellar cores - where they freeze out at densities higher than those found for CO and other C-bearing molecules. Therefore, N-bearing molecules are excellent tracers of these dense regions that are otherwise difficult to observe. In this present work, we choose NH₃ and study its interaction on grain surfaces - which is still poorly understood - in the presence of other species found on grain surfaces like H₂O, CO₂ and ¹³CO. We performed various types of experiments with the four species under conditions that mimic those found in pre-stellar cores and protoplanetary disks, paying close attention to the behaviour of NH₃ in each case. We also calculated the binding energy of NH₃ on two different types of water substrates-compact-Amorphous Solid Water Ice (c-ASW) and Crystalline Ice (CI). The main findings of our study are the following:

1. During the co-deposition of NH₃ with H₂O, we observe a delay in the desorption and lowering of the NH₃ desorption rate. Additionally, H₂O traps around 6% of NH₃ which is then released during the water phase change from amorphous to crystalline. On the other hand, when NH₃ is co-deposited with either ¹³CO or CO₂, we observe no such behaviour. However, this behaviour is observed once again when we add H₂O to the NH₃-¹³CO or NH₃-CO₂ mixture. In the NH₃-¹³CO-H₂O and the NH₃-CO₂-H₂O experiments, we observe roughly 5-9% of trapped NH₃ w.r.t water which is then released during the phase change of water from amorphous to crystalline.
2. We note that NH₃ has a range of binding energy values instead of a unique value, in agreement with recent theoretical calculations. On CI, we obtained NH₃-H₂O binding energy values in the range of 3780K-4080K. NH₃ is able to amorphise the substrate surface by disrupting the structural order of the surface of the ice via hydrogen bonding with H₂O. In the case of c-ASW, we obtained binding energies in the range of 3630K-5280K (for a pre-exponential factor set to A= 1.94 10¹⁵ s⁻¹ in both cases).
3. During the TP-DED experiments, the crystallisation of NH₃ is noticeably impacted in the presence of H₂O and CO₂. Furthermore, the desorption temperature of NH₃ increases significantly in their presence and it desorbs over a longer range of temperatures. There is also some trapping of NH₃ observed during the experiments. This indicates that NH₃ has no definite snow line and seems to be strongly influenced by these species. The trapping enables it to be stored on the dust grains and, thereby, be available at later times and/or be transported to higher temperatures (e.g., closer to the central protostar or towards the inner disk of more evolved young stellar objects) to form more complex molecules.

Acknowledgements. This work was funded by CY Initiative of Excellence (grant "Investissements d'Avenir" ANR-16-IDEX-0008), Agence Nationale de la recherche (ANR) SIRC project (Grant ANR-SPV202448 2020-2024), by the Programme National "Physique et Chimie du Milieu Interstellaire" (PCMI) of

CNRS/INSU with INC/INP co-funded by CEA and CNES, and by the DIM-ACAV+, a funding programme of the Region Ile de France.

References

- Amiaud, L. 2006, PhD thesis, thèse de doctorat dirigée par Lemaire, Jean-Louis Astrophysique Cergy-Pontoise 2006
- Boogert, A. A., Gerakines, P. A., & Whittet, D. C. 2015, *Annual Review of Astronomy and Astrophysics*, 53, 541
- Bossa, B., Theulé, P., Duvernay, F., Borget, F., & Chiavassa, T. 2008, *Astronomy and Astrophysics*, 492, 719
- Bossa, J.-B., Isokoski, K., De Valois, M., & Linnartz, H. 2012, *Astronomy & Astrophysics*, 545, A82
- Caselli, P., Benson, P. J., Myers, P. C., & Tafalla, M. 2002, *The Astrophysical Journal*, 572, 238
- Caselli, P., Bizzocchi, L., Keto, E., et al. 2017, *Astronomy & Astrophysics*, 603, L1
- Caselli, P., Pineda, J. E., Sipilä, O., et al. 2022, *The Astrophysical Journal*, 929, 13
- Caselli, P., Walmsley, C., Tafalla, M., Dore, L., & Myers, P. 1999, *The Astrophysical Journal*, 523, L165
- Cazaux, S., Carrascosa, H., Caro, G., et al. 2021, arXiv preprint arXiv:2110.04230
- Chaabouni, H., Diana, S., Nguyen, T., & Dulieu, F. 2018, *Astronomy & Astrophysics*, 612, A47
- Cheung, A. C., Rank, D. M., Townes, C. H., Thornton, D. D., & Welch, W. J. 1968, *Phys. Rev. Lett.*, 21, 1701
- Collings, M. P., Anderson, M. A., Chen, R., et al. 2004, *Monthly Notices of the Royal Astronomical Society*, 354, 1133
- Collings, M. P., Dever, J. W., Fraser, H. J., McCoustra, M. R., & Williams, D. A. 2003, *The Astrophysical Journal*, 583, 1058
- Congiu, E., Sow, A., Nguyen, T., Baouche, S., & Dulieu, F. 2020, *Review of Scientific Instruments*, 91, 124504
- Crapsi, A., Caselli, P., Walmsley, M. C., & Tafalla, M. 2007, *Astronomy & Astrophysics*, 470, 221
- De Jong, A. & Niemantsverdriet, J. 1990, *Surface Science*, 233, 355
- Dutrey, A., Guilloteau, S., & Guelin, M. 1997, *Astronomy and Astrophysics*, 317, L55
- Fehér, O., Tóth, L. V., Kraus, A., et al. 2022, *The Astrophysical Journal Supplement Series*, 258, 17
- Ferrero, S., Grieco, F., Ibrahim Mohamed, A.-S., et al. 2022, *Monthly Notices of the Royal Astronomical Society*, 516, 2586
- Germain, A., Tinacci, L., Pantaleone, S., Ceccarelli, C., & Ugliengo, P. 2022, *ACS Earth and Space Chemistry*
- Gorski, M., Ott, J., Rand, R., et al. 2018, *The Astrophysical Journal*, 856, 134
- He, J., Acharyya, K., & Vidali, G. 2016, *The Astrophysical Journal*, 825, 89
- He, J., Clements, A. R., Emtiaz, S., et al. 2019, *The Astrophysical Journal*, 878, 94
- He, J., Frank, P., & Vidali, G. 2011, *Physical Chemistry Chemical Physics*, 13, 15803
- Henning, T. & Semenov, D. 2013, *Chemical Reviews*, 113, 9016
- Keto, E. & Caselli, P. 2010, *Monthly Notices of the Royal Astronomical Society*, 402, 1625
- Kimmel, G. A., Dohnálek, Z., Stevenson, K. P., Smith, R. S., & Kay, B. D. 2001a, *The Journal of Chemical Physics*, 114, 5295
- Kimmel, G. A., Stevenson, K. P., Dohnálek, Z., Smith, R. S., & Kay, B. D. 2001b, *The Journal of Chemical Physics*, 114, 5284
- Kruczkiewicz, F., Vitorino, J., Congiu, E., Theulé, P., & Dulieu, F. 2021, arXiv preprint arXiv:2104.10464
- Martín-Doménech, R., Caro, G. M., Bueno, J., & Goesmann, F. 2014, *Astronomy & Astrophysics*, 564, A8
- Minissale, M., Aikawa, Y., Bergin, E., et al. 2022, *ACS Earth and Space Chemistry*, 6, 597
- Noble, J., Theule, P., Duvernay, F., et al. 2014, *Physical Chemistry Chemical Physics*, 16, 23604
- Öberg, K. I., Boogert, A. C. A., Pontoppidan, K. M., et al. 2011, *ApJ*, 740, 109
- Pagani, L., Bacmann, A., Cabrit, S., & Vastel, C. 2007, *A&A*, 467, 179
- Penteado, E., Walsh, C., & Cuppen, H. 2017, *The Astrophysical Journal*, 844, 71
- Pineda, J. E., Harju, J., Caselli, P., et al. 2022, *The Astronomical Journal*, 163, 294
- Poch, O., Istiqomah, I., Quirico, E., et al. 2020, *Science*, 367, eaaw7462
- Potapov, A., Theulé, P., Jäger, C., & Henning, T. 2019, *The Astrophysical Journal Letters*, 878, L20
- Qi, C., Öberg, K. I., Wilner, D. J., et al. 2013, *Science*, 341, 630
- Redaelli, E., Bizzocchi, L., Caselli, P., et al. 2019, *Astronomy & Astrophysics*, 629, A15

- Sandqvist, A., Hjalmarsen, Å., Frisk, U., et al. 2017, *Astronomy & Astrophysics*, 599, A135
- Scott Smith, R., Zubkov, T., & Kay, B. D. 2006, *The Journal of chemical physics*, 124, 114710
- Sipilä, O., Caselli, P., Redaelli, E., Juvela, M., & Bizzocchi, L. 2019, *Monthly Notices of the Royal Astronomical Society*, 487, 1269
- Smith, R. S., Huang, C., Wong, E., & Kay, B. D. 1997, *Physical review letters*, 79, 909
- Speedy, R. J., Debenedetti, P. G., Smith, R. S., Huang, C., & Kay, B. D. 1996, *The Journal of chemical physics*, 105, 240
- Suhasaria, T., Thrower, J., & Zacharias, H. 2015, *Monthly Notices of the Royal Astronomical Society*, 454, 3317
- Tafalla, M., Myers, P., Caselli, P., & Walmsley, C. 2004, *Astronomy & Astrophysics*, 416, 191
- Tafalla, M., Myers, P., Caselli, P., Walmsley, C., & Comito, C. 2002, *The Astrophysical Journal*, 569, 815
- Tinacci, L., Germain, A., Pantaleone, S., et al. 2022, *ACS Earth and Space Chemistry*, 6, 1514
- Viti, S., Collings, M. P., Dever, J. W., McCoustra, M. R., & Williams, D. A. 2004, *Monthly Notices of the Royal Astronomical Society*, 354, 1141

Appendix A:**Table A.1:** Additional experiments carried out to study the behaviour of ammonia with H₂O, ¹³CO and CO₂ but not included in the main text.

No.	Experiment	Ratio	Quantity Deposited
			(ML)
1	{NH ₃ + H ₂ O}	1:3	5(NH ₃), 16 (H ₂ O)
2	{NH ₃ + H ₂ O}	1:1	5 of each
3	{NH ₃ + CO ₂ + ¹³ CO}	1:3:15	7.4 (¹³ CO), 1.7 (CO ₂), 0.5 (NH ₃)
4	{NH ₃ + CO ₂ }	1:3	6 (NH ₃), 18 (CO ₂)

for a site with lower binding energy. Following this principle, at low dosages (< 1ML), peak desorption occurs at higher temperatures. As the dosage increases, this peak shifts to lower temperatures. Once every adsorption site on the substrate is occupied, the peak stops shifting to lower temperatures. At this stage, any other incoming NH₃ binds to another NH₃ already adsorbed on the surface, and the desorption then follows zeroth order kinetics. This can be seen as the increase in peak height (12 min curve and above) and the subsequent shifting of the curve towards higher temperatures. Our experiments obtain 1 ML for an exposure time higher than 8 minutes but lower than 12 minutes. Hence, we chose a time of 9 min, similar to the time we obtained for ¹³CO and N₂ under similar beam conditions.

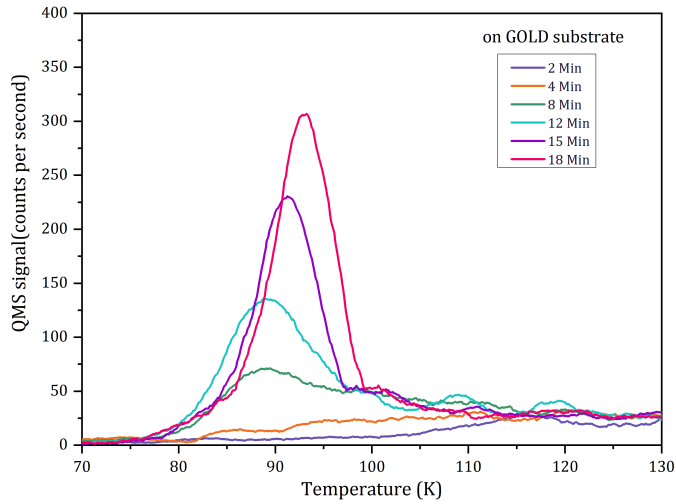
Appendix B:**Fig. B.1:** Experiments to calibrate for 1ML of NH₃. TPD curves of NH₃ deposited on a gold substrate for various dosages, used to calibrate for 1 ML. We use a constant flux of (insert value) and vary the duration of injection to vary the dosage.

Fig. B.1 shows the experiments performed to calibrate for 1 ML of NH₃. Varying doses of NH₃ are deposited onto the gold substrate at 10K, followed by a TPD. During deposition, adsorption sites with the highest binding energy are occupied first, followed by sites of lower binding energy until all the sites on the substrate are occupied. Hence, a species adsorbed on a site with higher binding energy will desorb at a higher temperature as opposed to desorption at lower temperatures